



# ALMA Unveils Widespread Molecular Gas Clumps in the Ram Pressure Stripped Tail of the Norma Jellyfish Galaxy

Pavel Jáchym<sup>1</sup>, Jeffrey D. P. Kenney<sup>2</sup>, Ming Sun<sup>3</sup>, Françoise Combes<sup>4</sup>, Luca Cortese<sup>5</sup>, Tom C. Scott<sup>6</sup>, Suresh Sivanandam<sup>7</sup>, Elias Brinks<sup>8</sup>, Elke Roediger<sup>9</sup>, Jan Palouš<sup>1</sup>, and Michele Fumagalli<sup>10</sup>

<sup>1</sup> Astronomical Institute, Czech Academy of Sciences, Boční II 1401, 14100, Prague, Czech Republic; [jachym@ig.cas.cz](mailto:jachym@ig.cas.cz)

<sup>2</sup> Department of Astronomy, Yale University, 260 Whitney Avenue, New Haven, CT 06511, USA

<sup>3</sup> Department of Physics and Astronomy, University of Alabama in Huntsville, 301 Sparkman Drive, Huntsville, AL 35899, USA

<sup>4</sup> Observatoire de Paris, LERMA, PSL, CNRS, Sorbonne Univ. UPMC, and College de France, F-75014, Paris, France

<sup>5</sup> International Centre for Radio Astronomy Research, The University of Western Australia, 35 Stirling Highway, Crawley, WA 6009, Australia

<sup>6</sup> Institute of Astrophysics and Space Sciences (IA), Rua das Estrelas, P-4150-762 Porto, Portugal

<sup>7</sup> Dunlap Institute for Astronomy and Astrophysics, University of Toronto, Room 101, 50 St. George Street, Toronto, ON M5S 3H4, Canada

<sup>8</sup> Centre for Astrophysics Research, University of Hertfordshire, College Lane, Hatfield AL10 9AB, UK

<sup>9</sup> Milne Centre for Astrophysics, Department of Physics & Mathematics, University of Hull, Hull, HU6 7RX, UK

<sup>10</sup> Institute for Computational Cosmology and Centre for Extragalactic Astronomy, Durham University, South Road, Durham DH1 3LE, UK

Received 2018 December 6; revised 2019 August 21; accepted 2019 August 25; published 2019 September 30

## Abstract

We present the first high-resolution map of the cold molecular gas distribution as traced by CO(2–1) emission with ALMA in a long ram pressure stripped tail. The Norma cluster galaxy ESO 137-001 is undergoing a strong interaction with the surrounding intracluster medium and is one of the nearest jellyfish galaxies with a long multiphase and multicomponent tail. We have mapped the full extent of the tail at 1'' (350 pc) angular resolution and found a rich distribution of mostly compact CO regions extending to nearly 60 kpc in length and 25 kpc in width. In total, about  $10^9 M_{\odot}$  of molecular gas was detected with ALMA. From comparison with previous APEX observations, we also infer the presence of a substantial extended molecular component in the tail. The ALMA CO features are found predominantly at the heads of numerous small-scale ( $\sim 1.5$  kpc) fireballs (i.e., star-forming clouds with linear streams of young stars extending toward the galaxy) but also large-scale ( $\sim 8$  kpc) superfireballs and double-sided fireballs that have additional diffuse ionized gas tails extending in the direction opposite the stellar tails. The new data help to shed light on the origin of the molecular tail; CO filaments oriented in the direction of the tail are likely young molecular features formed in situ, whereas large CO features tilted with respect to the tail may have originated from dense gas complexes that were gradually pushed away from the disk.

**Key words:** galaxies: clusters: individual (A3627) – galaxies: evolution – galaxies: individual (ESO 137-001) – galaxies: ISM – ISM: molecules – submillimeter: galaxies

## 1. Introduction

In recent years, numerous cluster galaxies with tails of ram pressure stripped (RPS) gas have been discovered, many containing young stars (e.g., Cortese et al. 2006; Sun et al. 2007; Yoshida et al. 2008; Hester et al. 2010; Smith et al. 2010; Yagi et al. 2013; Ebeling et al. 2014; Gullieuszik et al. 2017; Poggianti et al. 2017; Boselli et al. 2018). These are dramatic examples of galaxy evolution driven by the cluster environment in which ram pressure of the intracluster medium (ICM) efficiently strips star-forming cool interstellar matter (ISM) from infalling galaxies (Gunn & Gott 1972; Köppen et al. 2018). This causes star formation quenching of the main bodies of the galaxies (Koopmann & Kenney 2004; van Gorkom 2004) and their subsequent transformation toward early types.

Another aspect of ram pressure stripping of galaxies is the production of new young stellar components in the stripped ISM that join galaxy halos or intracluster space (Sun et al. 2007; Abramson et al. 2011; Fumagalli et al. 2011; Yagi et al. 2013; Kenney et al. 2014; George et al. 2018; Cramer et al. 2019; Poggianti et al. 2019). Young stars (ages  $< 10$  Myr) are found in the RPS tails at distances of up to several tens of kpc, indicating that they have formed in situ in the tails. Star formation in RPS tails provides a great opportunity to study the star formation process in a different environment from that in

galaxy disks, something that is not sufficiently well understood in galaxy evolution.

Tails of “jellyfish” galaxies are multiphase, containing gas with a wide range of densities and temperatures. They have been detected in X-rays (via bremsstrahlung from hot ionized gas; Finoguenov et al. 2004; Wang et al. 2004; Machacek et al. 2005; Sun & Vikhlinin 2005; Sun et al. 2006, 2010), H $\alpha$  (both from compact H II regions photoionized by young stars and from warm diffuse gas ionized by some other mechanism; Gavazzi et al. 2001; Yoshida et al. 2004, 2008; Cortese et al. 2006, 2007; Sun et al. 2007; Yagi et al. 2007, 2010; Fossati et al. 2012; Fumagalli et al. 2014; Boselli et al. 2016; Poggianti et al. 2017), and HI (emitted by cooler neutral gas; Kenney et al. 2004; Oosterloo & van Gorkom 2005; Chung et al. 2007, 2009; Scott et al. 2010; Abramson et al. 2011; Scott et al. 2012, 2018).

Recently, a cold molecular gas component was detected in several tails out to large “intracluster” distances from the galaxies (Jáchym et al. 2014; Verdugo et al. 2015; Jáchym et al. 2017; Moretti et al. 2018). In some cases, the molecular component was found to form an important or even dominant fraction of the tail gas mass (Jáchym et al. 2014, 2017). Other observations showed asymmetric or irregular molecular gas disks and off-disk molecular extensions in several cluster galaxies (e.g., Combes et al. 1988; Vollmer et al. 2001a, 2005; Vollmer et al. 2008; Dasyra et al. 2012; Scott et al. 2015;

Nehlig et al. 2016; Lee et al. 2017; Lee & Chung 2018; Zabel et al. 2019). In one sense, the presence of molecular gas in the tails is unsurprising, given that stars are forming there. On the other hand, explaining the presence of molecular clouds in RPS tails is not trivial, since molecular clouds, tracing the densest parts of the ISM, resist direct stripping more than any other constituent of the ISM. Moreover, the survival of molecular clouds in the intracluster environment is poorly understood.

We would like to understand the formation and evolution of star-forming molecular clouds in RPS tails. What are the roles of in situ formation versus direct stripping? Can stripped low-density gas cool sufficiently in the tails to produce dense gas and stars, or does ram pressure need to be strong enough to directly strip dense gas? How do molecular gas complexes in tails (their mass distribution, lifetimes, star formation efficiencies) compare to those in the disks of star-forming galaxies? How do star-forming molecular clouds evolve within the diverging gas flow of RPS tails? In order to make progress toward addressing these questions, we need high-resolution observations of molecular gas in the tails, a task that until now has not been possible.

We have obtained Atacama Large Millimeter/submillimeter Array (ALMA) CO(2–1) observations of ESO 137-001, a textbook example of a galaxy that is undergoing strong stripping by ram pressure. This allows us to study at subkiloparsec resolution the morphology and kinematics of the cold molecular gas component in a 60 kpc long RPS tail.

### 1.1. ESO 137-001

The galaxy ESO 137-001 in the Norma cluster (A3627;  $M_{\text{dyn}} \sim 1 \times 10^{15} M_{\odot}$ ,  $\sigma = 925 \text{ km s}^{-1}$ ) is one of the nearest “jellyfish galaxies” ( $z = 0.0163$ ), with a long X-ray,  $\text{H}\alpha$ , warm  $\text{H}_2$ , and CO tail, including young stars (Sun et al. 2006, 2010, 2007; Sivanandam et al. 2010; Fumagalli et al. 2014; Jáchym et al. 2014; Fossati et al. 2016). The presence of the one-sided gas tail, a strong HI deficiency of the main galaxy (Vollmer et al. 2001b), and an undisturbed stellar disk are clear characteristics of a ram pressure stripping interaction. The galaxy is projected at only  $\sim 14''.5 = 270 \text{ kpc}$  from the cluster center (assuming  $H_0 = 71 \text{ km s}^{-1} \text{ Mpc}^{-1}$ ,  $\Omega_M = 0.27$ ,  $1'' \approx 0.327 \text{ kpc}$ ). The tail is observed in its full extent thanks to a favorable projection on the sky; the galaxy’s radial velocity relative to the cluster mean is only about  $-200 \text{ km s}^{-1}$ , so its motion is mostly in the plane of the sky.

The multiphase ESO 137-001 tail is also a multicomponent system with a complex morphology; see the composite X-ray/ $\text{H}\alpha$  image in Figure 1. The central tail component that is brightest and longest in X-ray and  $\text{H}\alpha$  emission connects to the main body of the galaxy. It is rather narrow, with a width of  $\sim 15'' = 5 \text{ kpc}$  and a length of  $\sim 210'' = 70 \text{ kpc}$  and a slightly bent shape. In addition, there is also emission laterally beyond this central tail component. To the south, there is a secondary X-ray and  $\text{H}\alpha$  tail, which appears to originate outside the main body of the galaxy, above the stellar disk. To the north, there are some compact  $\text{H}\alpha$  sources (“orphan H II regions” with no associated diffuse X-ray emission) and patches of X-ray and  $\text{H}\alpha$  emission. This part of the tail shows no gaseous emission connecting it to the stellar disk, and there is also less diffuse ( $\text{H}\alpha$  and X-ray) emission between the sources than in the southern tail component. Since RPS generally acts from the outside in (see Section 3.4), the different parts are likely at different evolutionary stages of stripping.

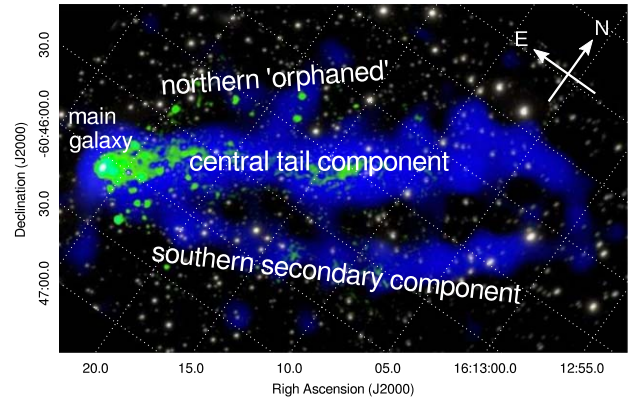


**Figure 1.** Composite X-ray *Chandra* (blue)/ $\text{H}\alpha$  SOAR telescope (green) image of ESO 137-001 (Sun et al. 2010) illustrating the multicomponent character of its RPS tail. The northern “orphaned” regions, central tail component, and southern secondary component are marked. Nearly all of the brightest optical sources are foreground stars. The image is rotated (note the N–E direction arrows) to match the orientation of the CO maps in Figure 2.

We used ALMA to observe all three tail components and nearly the full length of the (X-ray) tail; see the maps in Figure 2. In the present paper, we first describe the ALMA observations in Section 2 and compare them with CO(2–1) single-dish observations. We present in Section 3 maps of CO emission in ESO 137-001 and their comparison with ancillary data. We identify signatures of direct stripping and those indicating in situ formation in Section 4 and describe “fireball” features that are distinctive of ram pressure stripping in Section 5. Our conclusions are given in Section 6.

## 2. Observations

The observations were carried out with ALMA from 2016 January to July (Cycle 3 project 2015.1.01520.S; PI: Jáchym). Using Band 6 in dual polarization mode, a spectral window was centered at the CO(2–1) line at a sky frequency of 227.955 GHz in frequency division mode (FDM). The corresponding velocity resolution is  $\sim 0.64 \text{ km s}^{-1}$ . Three spectral windows were set to observe the continuum, centered at sky frequencies of  $\sim 229.746$ , 240.268, and 241.942 GHz. At  $\sim 228 \text{ GHz}$ , the half-power beamwidth (HPBW) of the primary beam of the telescope was about  $25''.7$ .

The main 12 m array observations were completed in six sessions, with the number of antennas varying in the range 38–49. The antennas were arranged in compact configurations with baselines in the range 15.1–469 m. To cover the main galaxy and most of the spectacular tail, a  $\sim 215'' \times 123''$  rectangular mosaic of 131 pointings was set. An average on-source time per pointing was  $\sim 1.9$  minutes. The median of the average system temperatures was 94 K.

Additional 7 m ACA array observations were obtained to increase the maximum recoverable spatial scale. In 15 observing sessions, 9–11 7 m antennas were used, with minimum and maximum baselines of 8.9 and 48.9 m, respectively. The largest recoverable scale is  $\sim 18''$  (calculated using the criterion of measuring 10% of the total flux density of a uniform disk; see the *ALMA Cycle 3 Technical Handbook*,

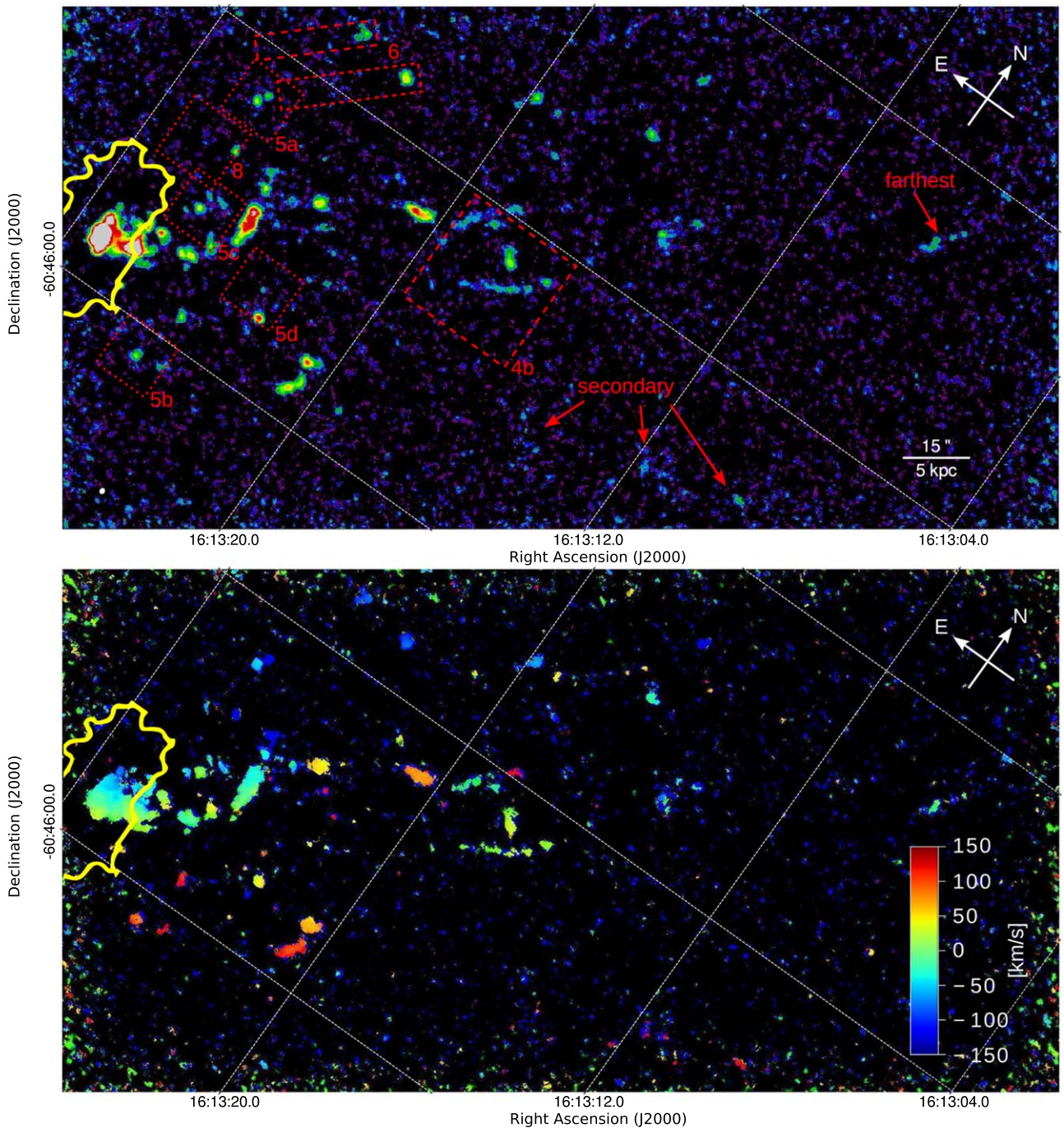


**Figure 2.** Integrated brightness map (top) and velocity field map (bottom) of the CO(2–1) emission in ESO 137-001 and its tail. The image is rotated (note the N–E direction arrows). The synthesized beam size is  $\sim 1''.4 \times 1''.2$ , i.e.,  $\sim 460 \text{ pc} \times 400 \text{ pc}$  (see the white dot in the lower left corner of the top panel). The outline of the optical disk is shown by drawing (yellow contour) the  $r$ -band isophote at  $22 \text{ mag arcsec}^{-2}$  (Fossati et al. 2016). Red dashed regions in the top panel mark the features displayed in Figures 4 (panel (b)), 5 (panels (a)–(d)), 6, and 8 and discussed in detail in Section 3. A couple of regions of interest are marked with arrows. The CO clumps are detected in all three tail components—the central tail, the northern “orphaned” regions, and the secondary southern component, where some mostly low signal-to-noise ratio emission regions are found out to  $\sim 30$ – $40 \text{ kpc}$  from the galaxy (see arrows). The edges of the mosaics where noise strongly increases due to the applied correction for primary beam attenuation are truncated.

Table 7.1). An average  $\sim 10$  minutes of on-source time was spent in each of 52 pointings covering the galaxy and its tail. The median of the average system temperatures was 75 K.

Flux calibration was based on observations of Titan, J1617–5848 (12 m and ACA), and J1427–4206 (ACA only). Bandpass calibration used J1427–4206 (12 m only) and J1924–2914 and J1517–2422 (ACA only), and the phase calibrator was J1617–5848.

The 12 m array and ACA data sets were calibrated separately with the ALMA pipeline. Using the CASA software package (v.4.5.3; McMullin et al. 2007), the continuum was subtracted in the  $uv$ -plane using the task `uvcontsub` first, followed by Briggs cleaning with a robust parameter of 0.5 and spectral smoothing to  $5 \text{ km s}^{-1}$ . The resulting synthesized beam in the ACA and ALMA image data cubes is  $\sim 7''.9 \times 4''.6$  (PA of  $88^\circ$ ) and  $\sim 1''.1 \times 1''.0$  (PA =  $46^\circ$ ), respectively. The two data

cubes were concatenated in a standard manner (after checking the ratio of the weights) using the CASA task `concatenate`. The rms noise levels in the line-free regions of the resulting data cube are  $\sim 2.2$  mJy beam $^{-1}$  in  $5$  km s $^{-1}$  channels. The final cube measures  $2048 \times 2048$  pixels of  $0''.14$  pixel $^{-1}$  and 64 channels of  $5$  km s $^{-1}$  width. The maps are corrected for primary beam attenuation.

In order to search for weak features, the maps presented in this paper were produced with a robust parameter of 2.0, thus close to natural weighting, which results in the lowest noise (highest signal-to-noise ratio). The resulting rms level is  $\sim 2$  mJy beam $^{-1}$ , and the synthesized angular resolution is  $\sim 1''.4 \times 1''.2$  (PA =  $58^\circ$ ). In order to create an integrated brightness CO(2–1) map, we explored different moment maps, but due to the high dynamic range of the data, many faint features stayed hidden in the noise. We therefore manually identified channels with maximum brightness in each pixel of the mosaic and integrated the spectrum only over a limited range of channels centered around the maximum channels (using the `astropy` python package; Astropy Collaboration et al. 2013). To determine the number of integrated channels, we identified the velocity widths of individual CO features and adapted the number of integrating channels accordingly. With this procedure, we were able to reach better results than with the standard moment maps. The velocity field map was constructed using an analogous method.

The uncertainties in the CO flux are estimated to be about 5%–20%. These include calibration uncertainties, CO flux errors arising from manually selecting the areas of the CO features, and the channels included in their integrated spectra.

### 2.1. Compact-to-extended Molecular Ratio

We use our previously obtained single-dish observations of ESO 137-001 with APEX (Jáchym et al. 2014) to make a direct comparison of the CO fluxes detected with APEX and ALMA in a number of common apertures. While in the main body of the galaxy, the APEX and ALMA fluxes are consistent (flux ratio of  $\sim 1.3$ ), in the tail regions, the APEX-to-ALMA ratio increases to values of 3–4. This suggests that while in the main body of the galaxy, both telescopes reveal about the same amount of CO-emitting gas, in the tail regions, the ALMA observations (which included ACA) resolve out  $\sim 67\%$ – $75\%$  of the CO emission. This is mainly due to missing total power observations and short spacings leading to a loss of extended, low surface brightness emission in the ALMA data. The RPS tail thus may be dominated by a diffuse, possibly warmer, subthermally excited molecular component (e.g., Pety et al. 2013) distributed on spatial scales larger than  $\sim 18'' \approx 6$  kpc, which is the largest recoverable scale in our ALMA observations. Moreover, the ratio of the APEX-to-ALMA fluxes increases with distance along the tail, implying that the fraction due to an extended component becomes larger further out in the tail.

We assume that for the compact features visible in the ALMA map and discussed further in this paper, the standard (Galactic) CO-to-H $_2$  conversion factor is applicable, while in the extended diffuse CO-emitting component, it may be a factor of a few lower (e.g., Bolatto et al. 2013). The uncertainty in the value of the conversion factor does not affect our conclusions. Assuming that the extended CO emission is distributed smoothly along the tail, it is likely that locally, the fraction of retrieved (compact) emission by ALMA is much

larger, possibly near 90%. The *Spitzer* IRS showed warm H $_2$  in the inner tail (Sivanandam et al. 2010). The origin of the diffuse molecular component and why it is supposedly stable against (gravitational) instabilities and thus does not form stars will be a matter for future studies.

## 3. Results

### 3.1. Overall CO Distribution and Kinematics and Relation to Tail Morphology

In Figure 2, we show the total CO(2–1) intensity and velocity maps of ESO 137-001 and its tail, and in Figure 3, we show the CO intensity overlaid on *Hubble Space Telescope* (*HST*) and H $\alpha$  images. In Figure 2, the maps are rotated (see the arrows indicating N and E). The RPS tail extends toward the right-hand side of the mosaic in a NW direction on the sky. Besides the bright CO-emitting molecular gas in the main body of the galaxy, the map reveals a rich distribution of mostly compact CO emission regions detected in the tail out to nearly 60 kpc distance from the disk and over a lateral extent of about 24 kpc. The CO clumps are associated with all three tail components: the northern “orphaned” regions, central tail, and secondary southern tail.

The CO emission in the main body of the galaxy is confined to the central region out to a radius of about  $4''$ – $5'' \sim 1.3$ – $1.6$  kpc (S–N). This is the region of the galaxy disk where stripping is currently active. The stellar disk beyond this radius has already been stripped (except in the north, where there is a CO clump at  $\sim 7''$  from the disk center). The amount of CO flux in the disk area (within a  $4'' \times 10''$  area centered along the disk) is  $\sim 43 \pm 5$  Jy km s $^{-1}$ . The integrated flux corresponds to an H $_2$  mass<sup>11</sup> of  $\sim 6.9 \times 10^8 M_\odot$  and an average face-on gas surface density within the central  $r = 1.5$  kpc of about  $150 M_\odot \text{pc}^{-2}$ . Such a surface density is typical for the center of gas-rich spirals and high enough to make the gas resistant to rapid ram pressure stripping.

Outside the main body, the brightest part of the tail is the central component, with a total CO integrated flux of  $57 \pm 10$  Jy km s $^{-1}$ , which corresponds to  $M(\text{H}_2) \sim 9.1 \times 10^8 M_\odot$ . It extends to  $\sim 58$  kpc from the disk. It is brightest in its innermost parts; within a mere 2.5 kpc adjacent to the disk, about 40% of the total CO flux is encompassed. By contrast, the lateral components of the tail contain much less molecular gas: the southern tail registers about  $9 \pm 2$  Jy km s $^{-1}$ , which is  $\sim 1.4 \times 10^8 M_\odot$  of H $_2$ , whereas the northern “orphaned” regions contain  $\sim 6 \pm 2$  Jy km s $^{-1}$ , i.e.,  $M(\text{H}_2) \sim 9.6 \times 10^7 M_\odot$ . Thus, about 80% of the detected total tail CO flux is in the central component, while small fractions of  $\sim 10\%$  are in the southern and northern regions. This indicates that the most important contribution to the molecular tail component comes from the relatively dense ISM most recently stripped from the central disk regions.

The total mass of the detected dense molecular gas in the tail is comparable to the total estimated X-ray gas mass of about  $\sim 10^9 M_\odot$  but larger than the upper limit estimate for neutral

<sup>11</sup> We follow the standard relation for the CO(1–0) luminosity of Solomon & Vanden Bout (2005) and assume a ratio of CO(2–1)-to-CO(1–0) of 0.8 (e.g., Leroy et al. 2009) and a CO/H $_2$  conversion factor of  $2 \times 10^{20}$  cm $^{-2}$  (K km s $^{-1}$ ) $^{-1}$  that is standard under the Milky Way disk conditions (e.g., Bolatto et al. 2013). A factor of 1.36 is included to account for helium.

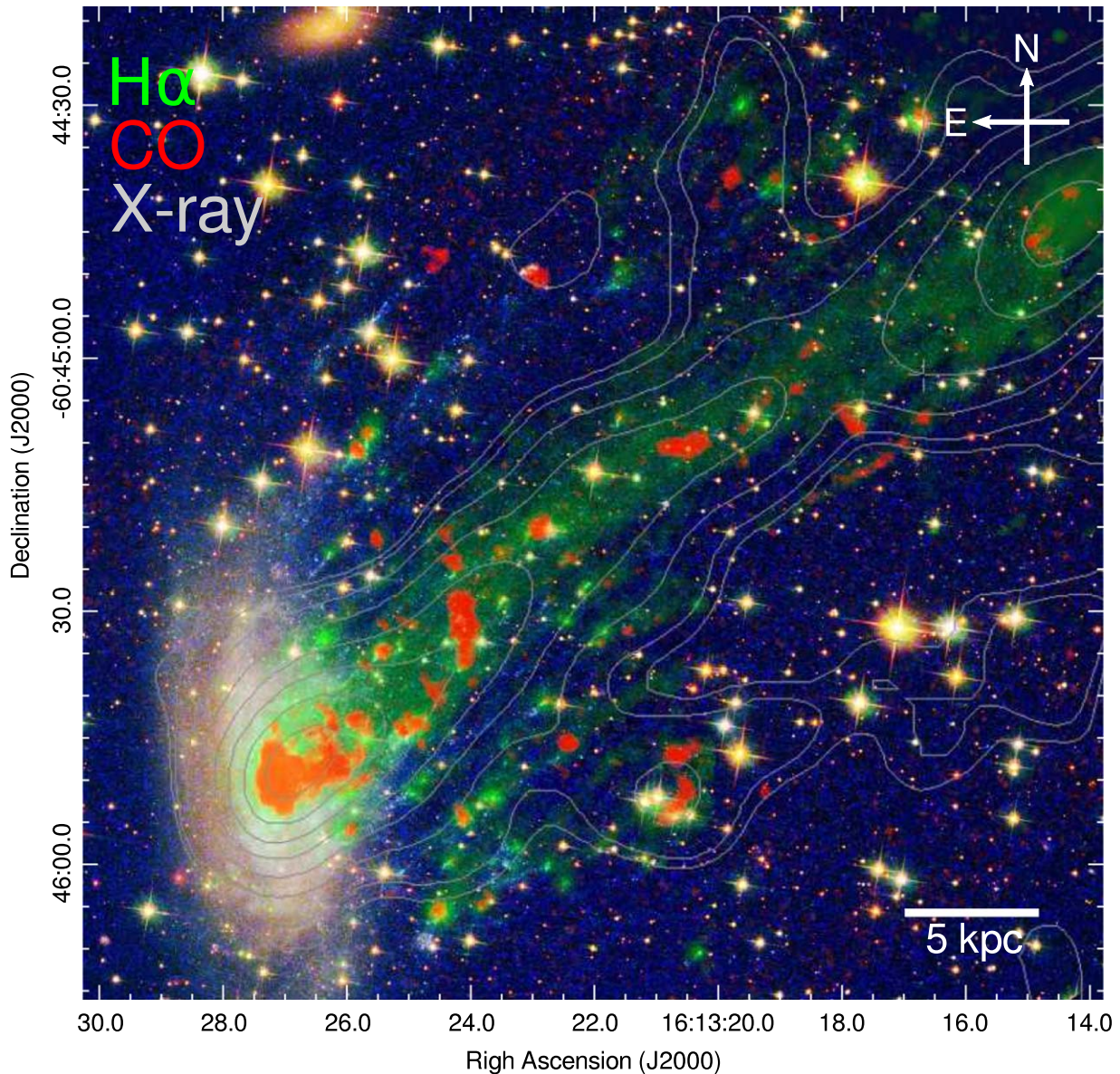


**Figure 3.** Overlay of ALMA CO(2–1) emission (red) on MUSE H $\alpha$  emission (green) and the *HST* WFPC3 image of ESO 137-001 (blue: F275W; green: F475W; red: F814W) with *Chandra* X-ray contours on top (Sun et al. 2010). North is up. Only the inner half of the (X-ray) tail is displayed. The upper left and lower right parts of the image were not covered by the MUSE observations (see Figure 2 in Fumagalli et al. 2014). The *HST* image reveals a highly inclined spiral galaxy disk ( $i \sim 66^\circ$ ) plus numerous complexes of blue recently formed stars to the west of the disk associated with parts of the RPS gas tail.

atomic gas of  $\sim 5 \times 10^8 M_\odot$  (Jáchym et al. 2014; Sun et al. 2006; Vollmer et al. 2001b).

The velocity structure shown in the bottom panel of Figure 2 is dominated by the galaxy’s rotation that is imprinted into the stripped gas: most of the northern emission regions are blueshifted relative to the tail centroid, while those in the south are mostly redshifted. Due to the galaxy’s orbital motion that is mostly in the plane of the sky, a velocity gradient along the tail is absent. A similar velocity structure was also reported from the early H $\alpha$  observations (Sun et al. 2010) and later confirmed from the detailed MUSE H $\alpha$  map (Fumagalli et al. 2014). The CO velocity dispersion is typically  $\sim 5\text{--}15 \text{ km s}^{-1}$  in most clumps but larger ( $\sim 15\text{--}25 \text{ km s}^{-1}$ ) in the galaxy and the brightest regions of the inner tail.

### 3.2. Compact Molecular Component of the Tail

The spatial resolution of the present ALMA observations of  $\sim 350 \text{ pc}$  does not allow us to resolve individual giant molecular clouds (GMCs) that in galaxies have typical sizes of the order of  $\sim 1\text{--}100 \text{ pc}$ . Besides some unresolved clumps, most of the detected CO emission regions in the tail of ESO 137-001 are larger structures, some with a clear sub-structure. Typical CO clumps have masses characteristic of GMCs or giant molecular associations (GMAs) of  $\sim 10^6\text{--}10^7 M_\odot$ , but their sizes (and also velocity dispersion) are larger ( $\sim 500\text{--}800 \text{ pc}$ ). This suggests that the clumps are not gravitationally bound and will likely disperse with time. For the selection of the CO clumps described in the present work, we can estimate their virial parameter  $\alpha$ . Following Bertoldi & McKee (1992),

$$\alpha = 5\sigma^2 R / (G M), \quad (1)$$

where  $\sigma$ ,  $R$ , and  $M$  are a clump’s velocity dispersion, radius, and mass, respectively (see the CO spectra in Figure 5). The parameter  $\alpha$  spans a range of  $\sim 2$ –12 that indicates subcritical structures (nonmagnetized clouds are expected to have critical virial parameters of  $\sim 2$ ; e.g., Kauffmann et al. 2013). This supports the abovementioned suggestion that molecular clumps will dissolve with time; however, the uncertainty of these estimates may be large. A detailed study of the molecular clump population detected in the ALMA data in the tail and its relationship to the star-forming regions will be the subject of a future paper. Also in the narrow RPS tail of the Coma galaxy D100, stellar sources were measured to be much larger than single gravitationally bound star clusters, indicating that they are likely to be unbound and disperse (Cramer et al. 2019).

### 3.3. Multiphase View of the RPS Tail

In Figure 3, the CO(2–1) intensity map (red) is overlaid with  $H\alpha$  (green) and *HST* UV–visible–near-IR composite images covering about the inner half of the length of the (X-ray) tail. Contours of X-ray emission are added into the overlay (Sun et al. 2010). The image indicates various levels of correlation between the CO,  $H\alpha$ , and young stars. It also clearly shows that the narrow central tail is connected to the CO-emitting molecular gas still in the central parts of the main body of the galaxy. The CO clumps detected outside the main body of the galaxy are associated with all tail components, but in comparison to the more extended  $H\alpha$  distribution, the CO emission comes from more compact regions. Given that the CO emission traces a relatively dense gas phase (see Section 2.1), the ALMA CO observations reveal for the first time the dense “skeleton” of the multiphase gaseous tail, as well as the component that forms the stars that are visible in the *HST* image. The overlay image in Figure 3 offers the most complete view of the spectacular RPS tail up to now, with the CO,  $H\alpha$ , and X-ray-emitting gas components, as well as the regions of young star formation.

### 3.4. Molecular Gas Tail Morphology and RPS History

The overall molecular gas distribution in the tail roughly follows the distribution of the other gas phases and reflects the stripping history of the disk. The lateral extent of CO in the tail is much broader than the lateral extent of CO in the disk. This is because RPS generally acts from the outside in, and outer disk gas is generally stripped earlier and forms the broadest parts of the tail. The broadest parts of the tail (the northern and southern components) originated from outer disk regions that were fully stripped some time ago. The kinematics support this with red- and blueshifted velocities in the parts of the tail furthest from the tail centroid (Figure 2).

The complex morphology of the multicomponent tail of ESO 137-001 is not consistent with the simple outside-in stripping. The continuous central long component of the tail that is also bright in CO and connects to the CO in the main body of the galaxy extends much further out than the innermost northern tail component, and it is also spatially separated from both the northern and southern components. This indicates that the central few kpc of the galaxy have been experiencing stripping at the same time as the outer disk. In a galaxy with ISM substructure, the ICM wind may penetrate through low-density parts of the disk, and multiple radii may be stripped

simultaneously (e.g., Quilis et al. 2000). This is what we think is likely happening in ESO 137-001.

The timescale of gas stripping depends on the galaxy’s orbit in the cluster, as well as on the gas column density. Assuming a cluster model with a virial mass and radius consistent with the measurements of Woudt et al. (2008) and the ICM distribution  $\beta$ -model fit to the *ROSAT* X-ray data of Boehringer et al. (1996), semi-analytic modeling indicates that ESO 137-001 is currently only  $\sim 100$  Myr before pericenter along a highly radial orbit with a large relative velocity  $> 3000$  km s $^{-1}$  and the corresponding peaked ram pressure time profile having a FWHM  $\sim 200$  Myr and current value  $P_{\text{ram}} = \rho_{\text{ICM}} v_{\text{orb}}^2 \approx 1.5 \times 10^{-10}$  dyne cm $^{-2}$  (Jáchym et al. 2014). For the range of column densities corresponding to the mean values of the typical CO clumps detected in the tail, we can calculate the distances along the tail to which stripped disk gas parcels have been pushed by the (face-on) ram pressure and their corresponding travel times. From, e.g., 2 kpc radius in the disk, a gas clump with a column density of 10 (20 or 30)  $M_{\odot}$  pc $^{-2}$  was pushed to 80 (20 or 7) kpc distance along the tail, with the corresponding travel time of 200 (90 or 50) Myr since the gas parcel crossed 1 kpc height above the disk midplane. From the outer disk radii, stripping has started much earlier along the orbit, and the stripped gas reaches much larger distances. These calculations neglect all hydrodynamic effects, as well as the internal structure of gas clouds.

The new observations also show the asymmetry between the northern and southern tail components. There are prominent isolated CO clumps in the northern tail occurring to nearly 40 kpc from the main galaxy, whereas in the southern tail, clumps are found only out to  $\sim 20$  kpc (with some marginal detections at larger distances). The asymmetry of the tail is likely caused by the effects of disk inclination with respect to the ram pressure direction. The interaction with the ICM wind is not face-on but tilted<sup>12</sup> by  $\sim 47^{\circ}$ , which means that the rotation of the galaxy has affected the trajectories of the stripped gas in an asymmetric manner: the gas on the northern disk side has a rotation velocity component pointing against the ICM wind, while the gas on the southern disk side rotates with the wind.

Thus, different parts of the tail are at different evolutionary stages of stripping: the central component is still being fed by the galaxy, while the outer, northern, and southern components represent later evolutionary stages, since these parts of the tail are no longer being fed from the galaxy. The northern tail component appears to be at a later evolutionary stage than the southern component, as it has less diffuse  $H\alpha$  and X-ray emission with isolated (“orphaned”) dense CO and  $H\alpha$  clumps apparently left behind the more diffuse gas. Despite their different ages, all three tail components are found to host molecular gas and young stars.

<sup>12</sup> The wind angle, i.e., the angle between the disk plane and the direction of the wind, has a value of  $\sim 47^{\circ}$ , following from the disk position angle ( $\sim 9^{\circ}$ ), the disk inclination angle ( $\sim 66^{\circ}$ ; HyperLEDA), the position angle of the tail ( $\sim 316^{\circ}$ ), and an assumption that the tail follows the past orbital path. The wind angle is thus a complementary angle between the wind vector  $\mathbf{w} = (\sin 44^{\circ}, \cos 44^{\circ}, 0)$  and the normal vector to the disk plane  $\mathbf{n} = (\cos 9^{\circ}, \sin 9^{\circ}, \cos 66^{\circ})$ .

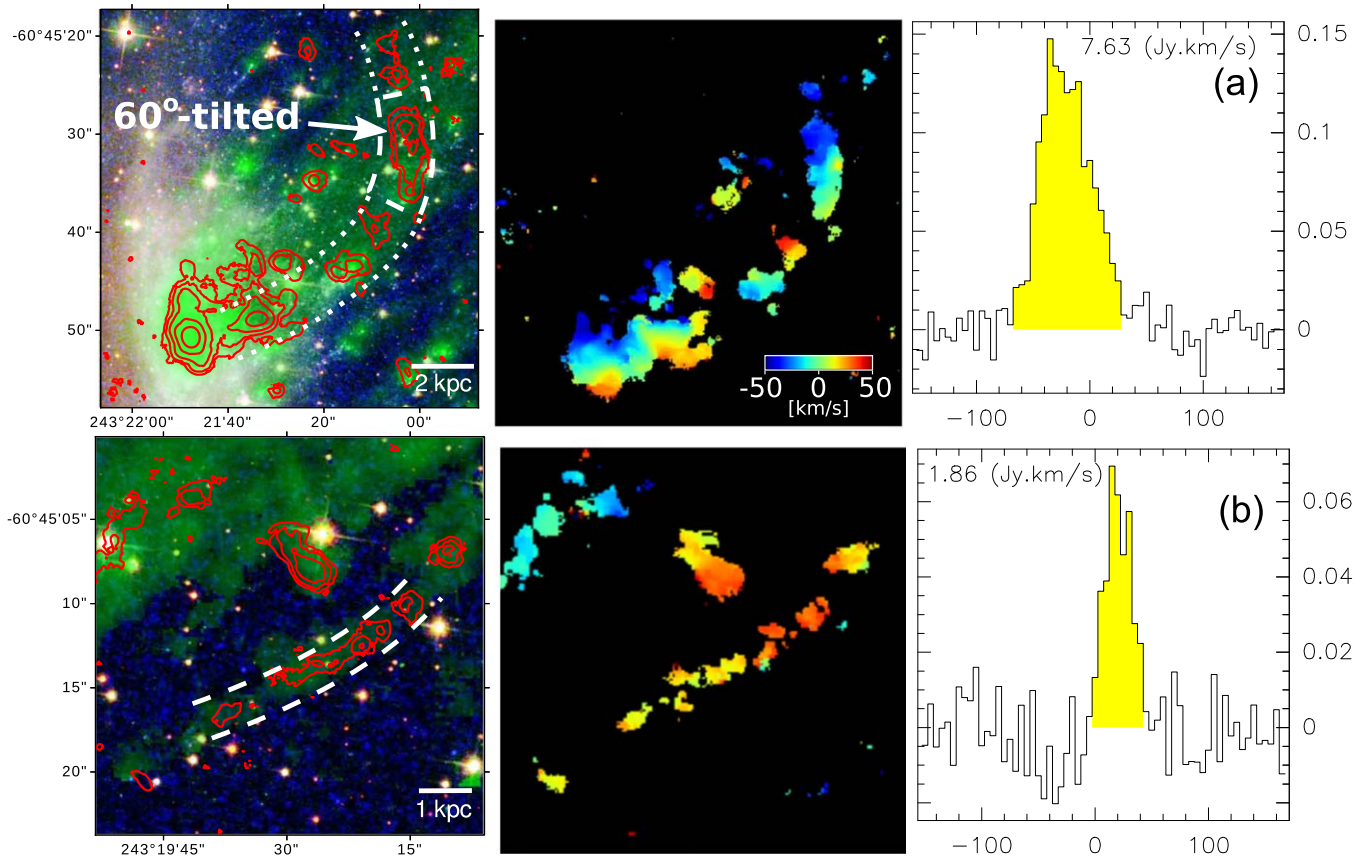


**Figure 4.** Large CO features found in the central tail component—the feature tilted  $60^\circ$  from the tail axis (top row) and the filamentary structure (bottom row)—shown in a composite *HST*-MUSE image with CO contours overlaid in red (left panels). North is up. The CO velocity maps and CO spectra integrated over the features are shown in the middle and right panels, respectively. The spectra’s units are  $\text{km s}^{-1}$  and Jy. Note that the top spectrum is integrated only over the  $60^\circ$  tilted clump, not the full dotted area indicated in the left panel. The CO contour levels are 0.12, 0.32, 0.79, 1.9, and 5.0 (top) and 0.11, 0.17, 0.28, and 0.44 (bottom)  $\text{Jy beam}^{-1} \text{ km s}^{-1}$ .

#### 4. Origin of Large Molecular Structures Detected in the Tail

In the following section, we focus on several distinct features that may prompt a new perspective on the origin and evolution of dense gas in the stripped ISM. Two physical scenarios are usually considered: either the molecular gas has formed in situ out of stripped atomic gas (in situ formation) or some preexisting molecular gas contributed to it (direct stripping). The central tail component is in the earliest evolutionary stage, in the sense that gas is still being fed to it from the main galaxy. We therefore might expect to find within it molecular gas concentrations at relatively early evolutionary stages, including some that have recently formed. We describe two distinct CO complexes in the central tail, one of which may have formed from a large gas structure originating in the galaxy disk and another that may have formed in situ.

##### 4.1. Large Feature Tilted $\sim 60^\circ$ from the Tail Axis

At about 9.5 kpc from the galaxy, we find an extended bright CO feature that is tilted  $\sim 60^\circ$  from the tail axis (see the CO velocity field and integrated CO spectrum in Figure 4, top panels), nearly parallel to the main disk. It is about  $10''$  long and  $3''.5$  wide ( $\approx 3.3 \text{ kpc} \times 1.1 \text{ kpc}$ ). Its total integrated flux is  $8 \pm 1 \text{ Jy km s}^{-1}$ , corresponding to  $\sim 1.3 \times 10^8 M_\odot$ . The velocity of the structure ranges from  $\sim -50$  to  $20 \text{ km s}^{-1}$ , with a gradient along its length in the N–S direction.

The feature may be part of a longer structure that extends through the inner tail and bends upward (see dotted lines in Figure 4). The fact that it is tilted at a large angle with respect to the main tail direction and is possibly connected to the gas in the galaxy strongly suggests it originated from a large dense gas complex in the galaxy, such as a spiral arm, that was gradually removed from the disk by ram pressure. The reason is that the flow in the downstream direction naturally makes elongated gas features in the tail direction but does not naturally create structures oriented at an angle to the tail direction. To directly entrain dense, large clumps, dynamical effects can help. In a tilted ram pressure orientation, some larger structures may have a rotation velocity component in the direction of the wind, and in combination with a locally enhanced gravitational potential (e.g., by overdensities in spiral arms), they may be pushed gradually by the wind instead of being disrupted.

The  $60^\circ$  tilted feature is an example of a dense structure of the RPS tail that remained hidden in the previous observations; neither  $\text{H}\alpha$  nor X-rays show an associated coherent structure, and there is also no excess of young stars. In Section 3.4 we estimated that a gas clump with the column density of  $30 M_\odot \text{ pc}^{-2}$  at 2 kpc disk radius has been pushed to  $\sim 7$  kpc from the disk in the last 50 Myr. Despite the simplicity of the model, it matches well the mean column density ( $\sim 35 M_\odot \text{ pc}^{-2}$ ) and location of the  $60^\circ$  tilted feature and thus indicates that the (stripping) age of the feature is  $\sim 50$  Myr. This time also corresponds to (less than) half of the galaxy rotation

period (for a galaxy rotation velocity of  $\sim 110 \text{ km s}^{-1}$ ; Jáchym et al. 2014). The observed shape of the CO structure connecting the  $60^\circ$  tilted feature to the main galaxy that is not twisted but forms a single arc is consistent with this evolutionary path.

The main issue for the direct stripping scenario is the survival of molecular clouds in the presence of the disruptive effects of the hot ICM wind, notably to the Kelvin–Helmholtz (KH) and Rayleigh–Taylor instabilities. The crushing time of a cloud with a radius  $r_{\text{cloud}}$  in a wind with a speed  $v_{\text{wind}}$  can be approximated by the time it takes for a shock to propagate through the cloud (Klein et al. 1994),

$$t_{\text{cc}} = \chi^{1/2} \frac{2 r_{\text{cloud}}}{v_{\text{wind}}}, \quad (2)$$

where  $\chi$  is the density contrast between the cloud and the wind. For clouds with parameters of typical GMCs, the crushing time due to an  $\sim 1000 \text{ km s}^{-1}$  wind is rather short,  $\sim 10^7 \text{ yr}$ . For larger clumps, it is longer,  $> 10^8 \text{ yr}$ , which is comparable to their travel (drag) time to the inner regions of the tail by ram pressure. Some physical processes may protect the clouds and prolong their lifetime, such as magnetic fields that reduce the growth rate of the KH instability (e.g., Kauffmann et al. 2013). Also, radiative cooling effectively extends the lifetime of dense clouds by replenishing the cold gas and preventing complete mixing with the hot wind (e.g., Cooper et al. 2009). Since the cooling time is shortest for the densest gas, it will be the densest stripped gas clouds or clouds compressed by RP that will form most of the extraplanar molecular clouds in the inner parts of the tail, such as the  $60^\circ$  tilted feature.

It is thus possible that direct stripping is a viable scenario for the origin of the CO-bright large features observed in the inner parts of the tail, close to the main galaxy. This is consistent with the continuous connection of the CO emission in the base of the tail to the galaxy. Dense molecular clouds may be embedded in large reservoirs of more diffuse molecular ISM (Pety et al. 2013), which further protect them against the disruptive effects of ram pressure and may itself be directly stripped (see Section 2.1).

#### 4.2. Large Feature Parallel to the Main Tail, with Clumpy Substructure

Another large CO feature in the central tail component is a linear structure located at nearly 30 kpc from the galaxy, somewhat south of the central tail (Figure 4, bottom panels). It is longer and thinner, has more substructure than the  $60^\circ$  tilted feature, and, most substantially, is parallel to the main tail direction. Along its length of  $\sim 18'' \approx 6 \text{ kpc}$ , at least eight clumps are identified. Some of the clumps are resolved, but the width of the feature is mostly unresolved at  $\sim 1''$ . The total CO flux of nearly  $2 \text{ Jy km s}^{-1}$  corresponds to  $\sim 3.2 \times 10^7 M_\odot$ . The masses of individual clumps are typically  $\sim 2.5\text{--}5 \times 10^6 M_\odot$ . Their characteristic separation in the filament is  $\sim 2'' \approx 0.5\text{--}0.6 \text{ kpc}$ . The radial velocity range of the structure is  $\sim 0\text{--}40 \text{ km s}^{-1}$  with no apparent velocity gradient along its length (although the inner half is at a somewhat lower velocity than the outer half).

While there is diffuse  $\text{H}\alpha$  observed along the entire feature, there are virtually no young stars or associated compact  $\text{H}\alpha$  peaks. This implies that the CO filament is relatively young, unevolved with respect to star formation. Moreover, it is located far from the galaxy and oriented parallel to the main

tail. These characteristics make it consistent with a dense gas filament formed recently in situ in the tail from a less dense gas. It then fragments via a gravitational instability, forming a regular substructure of molecular clumps, which may eventually form new stars. Thanks to the offset location from the main part of the central tail, the CO filament is a particularly clear example of a possible in situ formation.

From the theory of fragmentation of self-gravitating isothermal, hydrostatic cylinders, following the analysis in, e.g., Mattern et al. (2018), we can estimate the most unstable scale,

$$\lambda_{\text{max}} = \frac{22 c_s}{\sqrt{4\pi G \rho_c}}, \quad (3)$$

where  $\rho_c$  is the central density of a filament in virial equilibrium,  $c_s = \sqrt{k_B T / \mu m_H}$  is the sound speed, and  $T$ ,  $\mu$ , and  $m_H$  represent the isothermal temperature, mean molecular weight, and mass of the hydrogen atom, respectively. For the mean density calculated for individual clumps from their masses ( $\sim 2.5 \times 10^6 M_\odot$ ) and sizes ( $\sim 350 \text{ pc}$ ), and assuming  $T = 15 \text{ K}$  to calculate the sound speed, the corresponding fragmentation length scale is  $\sim 250 \text{ pc}$ , which is within a factor of  $\sim 2\text{--}3$  consistent with the observed clump separation in the filament. The predicted value would be higher and thus better match the observed separation when a turbulent medium is assumed, in which the velocity dispersion is higher than the sound speed. While these estimates are strongly simplified by neglecting the presence of an external pressure, rotation, magnetic fields, and by using mean densities, they suggest that fragmentation due to self-gravity is taking place in the stripped gas.

In addition to the central filamentary structure, the most distant CO emission region detected at about 58 kpc from the galaxy also has a linear morphology. It is shorter; composed of at least three clumps with a total integrated flux of  $\sim 1 \text{ Jy km s}^{-1}$ , thus about  $1.6 \times 10^7 M_\odot$ ; and is oriented roughly along the tail direction (see Figure 2). The flow of matter in the downstream direction naturally creates elongated gas features in the tail direction that may eventually cool down, condense, and fragment. The two CO filamentary structures may provide the first direct evidence for molecular gas formation in situ in RPS tails.

The importance of the scenario of molecular gas formation in the tail is also supported by the large total amount of molecular gas revealed in the tail in the present observations (plus taking into account the more extended component; see Section 2.1). Following the scaling relations of, e.g., Catinella et al. (2018), for an unperturbed galaxy with a stellar mass  $\sim 10^{10} M_\odot$ , the expected total gas fraction is  $\sim 0.3$ , and the molecular-to-atomic gas mass ratio is  $\sim 0.2$ ; thus, the estimated pre-stripping  $\text{H}_2$  content of ESO 137-001 is  $\sim 5 \times 10^8 M_\odot$ . While such estimates may vary by almost an order of magnitude at a fixed stellar mass, this value is well consistent with the detected amount of  $\sim 7 \times 10^8 M_\odot$ . This suggests that the galaxy is not  $\text{H}_2$ -deficient. But it is strongly H I-deficient, following an expected pre-stripping H I content of  $\sim 2.5 \times 10^9 M_\odot$  and a weak upper limit obtained from Australia Telescope Compact Array observations of  $\sim 5 \times 10^8 M_\odot$  (Vollmer et al. 2001b). Thus, there was, in principle, enough stripped H I to account for the observed  $\text{H}_2$  content.



Recent simulations of the evolution of cold ( $\sim 10^4$  K) gas in a hot galactic wind have shown that if the cooling is fast ( $t_{\text{cool}} \ll t_{\text{cc}}$ ) and the clouds are sufficiently large, they can withstand longer mixing times due to the KH instability, and new cold gas may form far downstream from the clouds from a “warm” mixture of the cold gas and hot wind (Gronke & Oh 2018). Moreover, in the simulations, the amount of newly formed cold gas may exceed the original cold gas in the clouds. Assuming that the  $\sim 10^4$  K gas in the simulations can cool further down to reach the typical temperatures of molecular gas, this process could help to understand the origin of the large total  $\text{H}_2$  content of ESO 137-001.

In order to turn the stripped cold gas (HI) into a molecular phase, the presence of dust is crucial. Imaging of the galaxy with *HST* clearly shows prominent dust features on the west side of the disk and the inner tail. In addition, *Herschel* SPIRE imaging (S. Sivanandam et al. 2019, in preparation) reveals a dust trail emanating from the galaxy in the direction of the gas tail. Other optical observations (e.g., *HST*) of RPS galaxies clearly show dust being stripped from the galaxies along with the gas (Elmegreen et al. 2000; Abramson et al. 2016; Cramer et al. 2019).

Interestingly, the physical scenarios of direct stripping and in situ formation are also relevant for galactic winds, which can have a cold gas component associated with the hot gas in outflows (see, e.g., Banda-Barragán et al. 2019), and for brightest cluster galaxies, which can have molecular gas filaments extending radially from the galaxies (e.g., Vantyghe et al. 2019).

## 5. Dynamical Separation of Gas from Newly Formed Stars in the Tail

Within the tail, the degree of correlation between individual gas phases and star formation varies (Figure 3). One can find examples of CO clumps with and without young stars or H II regions, and vice versa. Much of this variety is likely due to different evolutionary stages of star formation. While a similar large range in CO/young star ratios can be found in normal galaxies, the distribution of the features in the tail and their morphology are particular and characteristic to RPS tails. This is caused by dynamical separation: denser, more compact (molecular) clumps are less accelerated by ram pressure and lag behind more diffuse gas. Newly formed stars decouple from the surrounding gas, and if they have not reached the escape velocity, they fall back toward the galaxy. The effects of differential acceleration of individual phases of the stripped ISM by ram pressure were indicated previously from observations (e.g., Vollmer et al. 2008; Jáchym et al. 2017).

Numerous linear streams of young blue stars of different lengths parallel with the tail direction that are distributed in all three tail components are visible in the *HST* image (see Figure 3). The ages of the young star clusters range from a few Myr to  $\sim 100$  Myr and are consistent with formation in the tail after stripping. The details of the star formation in the tail, including the age distribution of the star clusters, will be discussed in M. Sun et al. (2019, in preparation). Some stellar and gaseous features are physically linked, forming fireballs, star-forming clouds with a linear stream of young stars extending toward the galaxy. Fireballs were previously observed in several RPS galaxies (Cortese et al. 2007; Yoshida et al. 2008, 2012; Kenney et al. 2014). A simple model of fireballs was introduced by Kenney et al. (2014).

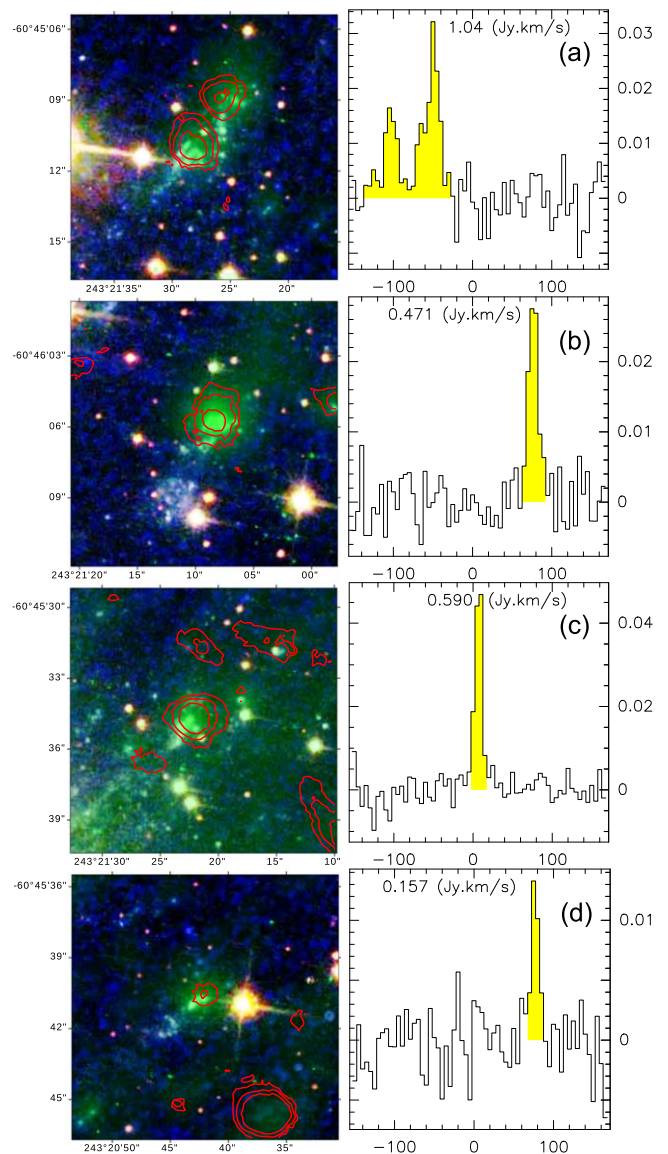


**Figure 5.** Examples of small-scale fireballs—linear streams of young stars with molecular clouds at their heads—from all three tail components (see their locations in Figure 2, marked with small dashed squares). Left panels: CO contours (red) and  $\text{H}\alpha$  emission (green) overlaid on an *HST* image (north is up). The CO contour levels are 0.11, 0.17, 0.28, and 0.44  $\text{Jy beam}^{-1} \text{ km s}^{-1}$ . The molecular “heads” are associated with compact  $\text{H}\alpha$  (H II) regions. The size of the panels is  $\sim 11 \times 11 \text{ arcsec}^2$ , i.e.,  $\sim 3.6 \times 3.6 \text{ kpc}^2$ . Right panels: CO integrated spectra of the central CO features (except the top panel, where a spectrum integrated from both CO clumps is shown).

### 5.1. Fireballs: Linear Streams of Young Stars with Molecular Clouds at Heads

In all three tail components, one finds CO clumps with offset small streams of young stars extending toward the galaxy. Four examples of fireballs are shown in Figure 5. The stellar streams have lengths of  $\sim 1''.5\text{--}4''.5$ , i.e.,  $\sim 0.5\text{--}1.5 \text{ kpc}$ , and are all oriented roughly parallel to the tail direction. The CO clumps at the heads of the fireballs are associated with compact  $\text{H}\alpha$  (H II) regions. Some components of fireballs ( $\text{H}\alpha$  and young stars) have previously been observed, but this is the first time the important molecular component has been detected.

Figure 5 also shows integrated CO spectra of the clumps at the heads of fireballs. The integrated CO fluxes are typically  $\sim 0.5 \text{ Jy km s}^{-1}$ , thus about  $8 \times 10^6 M_{\odot}$ , but some are fainter,

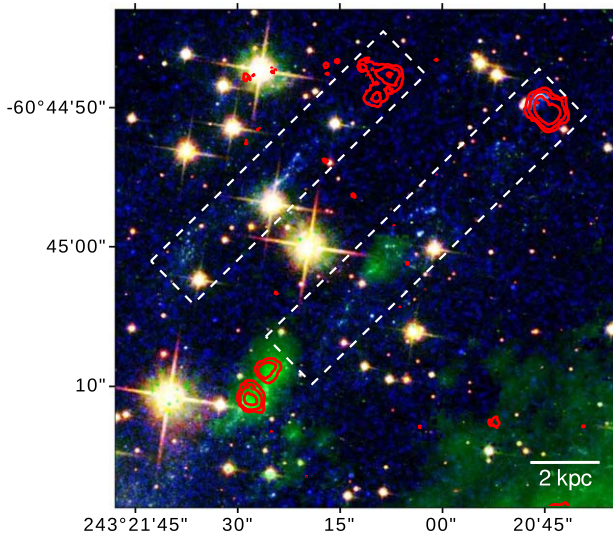


**Figure 6.** Large-scale fireballs (superfireballs) in the northern component of the tail. The CO contours (red; 0.12, 0.20, and  $0.32 \text{ Jy beam}^{-1} \text{ km s}^{-1}$ ) are overlaid on  $\text{H}\alpha$  (green) and a background *HST* image.

with an integrated CO flux of  $\sim 0.16 \text{ Jy km s}^{-1}$ , i.e.,  $2 \times 10^6 M_{\odot}$ . The typical sizes of the CO clumps are  $\sim 2''$ – $2''.5 \approx 650$ – $800 \text{ pc}$ , but some are smaller,  $\sim 500 \text{ pc}$ . Line widths are  $10$ – $15 \text{ km s}^{-1}$ . Many other fireballs in the tail have compact  $\text{H}\alpha$  clumps at their heads but no detected CO emission, similar to fireballs observed previously in other galaxies. This may indicate a different evolutionary stage in which molecular gas has already been consumed by star formation.

While we cannot measure the velocity structure of the fireballs due to the orientation of the orbit of ESO 137-001 in the plane of the sky, it is clear that their kinematics evolves with time. It depends on the timescales of ram pressure acceleration, gravitational acceleration from the galaxy, cloud condensation, and star formation. The newly formed stars gradually decouple from the gas clump and may eventually start falling back toward the galaxy if they have not reached the escape speed. Simple modeling with a realistic time-varying ram pressure and a galactic potential (adopted from Jáchym et al. 2014) shows that a separation of  $\sim 1 \text{ kpc}$  between the parent gas cloud and a decoupled star (modeled as a high column density parcel) typically establishes within (a few)  $10 \text{ Myr}$ . Thus, the observed fireballs (including those shown in Figure 5) are most likely dynamically young structures with molecular clumps at their head that have been actively forming new stars over the past  $\sim 10 \text{ Myr}$ .

### 5.2. Superfireballs

In the northern component of the tail, close to the disk, we find possible examples of much larger fireballs. In this part of the tail, which likely is in a later evolutionary stage of stripping, there is no diffuse X-ray or  $\text{H}\alpha$  emission but distinct streams of young stars, H II regions (compact  $\text{H}\alpha$  sources), and bright CO clouds. Most of the young stars seen in the *HST* image in this region fall within two linear streams  $\sim 15''$ – $25'' \approx 5$ – $8 \text{ kpc}$  in length, parallel to the main tail (see a closeup in Figure 6).

Each of these streams have CO clouds coincident with or somewhat beyond the outermost stars (in the downstream direction). This is consistent with the fireball scenario. The CO clouds have diameters of  $\sim 2''$  and  $4''$ , i.e.,  $\sim 650$  and  $1300 \text{ pc}$

(but with possible substructure); their line widths are  $\sim 22$  and  $30 \text{ km s}^{-1}$  and  $\text{H}_2$  masses  $\sim 6.4 \times 10^6$  and  $1.9 \times 10^7 M_{\odot}$ , respectively, for the E and W structures. The long streams do not have young stars extending continuously to the CO cloud or along the length of the streams. This indicates that molecular clouds in tails may survive after a period of active star formation ends and possibly go through several more phases of star formation activity. This is consistent with the subcritical values of the virial parameter  $\alpha$  of the detected CO clumps (see Section 3.2) if the clumps have denser substructures, unresolved by our present observations. Then the smaller fragments of otherwise dispersing clumps could survive, and some of them could eventually condense into star-forming regions. For example, the western fireball shows an  $\text{H}\alpha$  compact feature (with no detected associated CO emission) in its inner half. If not simply due to the effects of projection, this could correspond to a previous episode of condensation when denser (pre-stellar) fragments decoupled from a parental clump. The latter continued to be accelerated further by ram pressure in the downstream direction and condensed again only recently. The multiple features are then parts of one large-scale structure. In this picture, small-scale fireballs can, in fact, be part of large-scale fireballs. We note that the locations of the two CO clumps at the heads of the large fireballs lay outside the MUSE area, but previous Southern Observatory for Astrophysical Research (SOAR) observations show bright compact  $\text{H}\alpha$  emission associated with at least the western CO clump (Sun et al. 2007).

Superfireballs, due to their lengths, are expected to be dynamically older structures than the small-scale fireballs. This is consistent with their location in the northern outer tail component. Our modeling (described in Section 5.1) shows that  $\sim 50 \text{ Myr}$  is needed to develop a separation of  $\sim 10 \text{ kpc}$  between the parent cloud and decoupled stars. We may also be seeing superfireballs in the process of formation in the southern tail component. There, the sensitive MUSE  $\text{H}\alpha$  observations reveal many elongated structures (see Figure 3), some of which show a head–tail morphology, with diffuse tails extending away from the galaxy and compact clumps at the heads situated closer to the galaxy (sometimes associated with CO emission). Some are aligned into long coherent structures encompassing other  $\text{H}\alpha$  compact clumps. It is possible that with ongoing ram pressure, the diffuse component will be cleared out of the structures and moved downstream along the tail, leaving behind “nude” structures of denser clumps and stellar streams, i.e., superfireballs.

### 5.3. Double-sided Fireballs

Some of the  $\text{H}\alpha$  head–tail features in the tail are identified to be interconnected with fireballs. In addition to the Kenney et al. (2014) model, the tail of ESO 137-001 indicates that the fireballs may be double-tail features, with a second, gaseous tail of diffuse ( $\text{H}\alpha$ ) gas that is ablated from the dense star-forming clump that extends in the opposite direction to the stellar tail, away from the galaxy. The central dense clump of a fireball is bright in  $\text{H}\alpha$  and possibly also in CO emission. A cartoon of the model of the double-sided fireballs is shown in Figure 7. Similar features of considerable lengths were previously found in the RPS tail of the Coma galaxy RB199 (Yoshida et al. 2008), although without any associated molecular component yet observed.

An example of a double-sided fireball is given in Figure 8, which shows a compact H II region associated with a (slightly

## 6. Conclusions

We observed with ALMA in CO(2–1) the RPS tail of the Norma cluster galaxy ESO 137-001, one of the nearest jellyfish galaxies. The observations at  $\sim 1'' \approx 350$  pc resolution covered nearly the full extent of the multicomponent H $\alpha$  and X-ray tail: the central tail, northern “orphaned” regions, and southern tail component. The new high-resolution map of the cold molecular gas, together with observations at other wavelengths (*HST*, *Chandra*, VLT/MUSE), offers the most complete view of the spectacular RPS tail to date. The main results of a first analysis of the CO map and a comparison with observations at other wavelengths are as follows.

The CO emission arises from a rich distribution of mostly compact clumps detected in the tail out to nearly 60 kpc distance from the disk and over a lateral extent of about 24 kpc. The CO clumps are associated with all three components of the tail that are likely in different evolutionary stripping stages.

Most of the detected CO clumps in the tail are larger structures with masses of Galactic GMCs and GMAs but sizes and line widths that are larger than is typical of those found in the Galaxy. Estimates of their virial parameters indicate that the molecular clumps are not gravitationally bound and will disperse with time. The CO velocity field in the tail is dominated by the galaxy’s rotation that is imprinted into the stripped gas. Most of the northern regions are blueshifted, while those in the southern tail component are mostly redshifted relative to the tail centroid.

In total,  $\sim 9 \times 10^8 M_{\odot}$  of H $_2$  was revealed in the tail, assuming the standard Galactic CO-to-H $_2$  conversion factor. Comparison of fluxes of the ALMA+ACA observations with previous single-dish (APEX) observations indicate that, in addition to the compact CO features, there is a substantial component of extended (scales  $> 18''$ ) molecular gas in the tail. Its fraction increases with distance from the parent galaxy. The galaxy ESO 137-001 is molecular rich—the total amount of H $_2$  detected in the galaxy and the tail likely exceeds the pre-stripping molecular content of the galaxy.

From the morphology of some CO features, we can infer their origin in the tail. For example, filamentary structures oriented parallel to the tail direction and located at large distances from the disk have likely formed in situ through fragmentation via gravitational instability. Other CO features, such as the large clump in the inner central tail tilted  $\sim 60^\circ$  from the tail axis, may have formed from dense gas clumps, such as a spiral arm, stripped gradually from the disk. These CO features do not form distinct structures in H $\alpha$  or X-ray emission, and there is also no associated excess of young star formation. Simple analysis estimates their ages to  $\sim 50$  Myr.

The overall CO distribution in the tail roughly follows the distribution of the other gas phases and the regions of young star formation, but at small scales, the degree of correlation varies. It is the distribution of the features and their morphology that is particular and characteristic to RPS tails. Numerous “fireball” features with CO clumps at the heads and tails of young stars (typically  $\sim 1.5$  kpc) pointing toward the main galaxy are found in all three tail components. Newly formed stars decouple from the surrounding gas; those in the outer tail probably escape from the galaxy, but the inner tail stars fall back onto the galaxy, leading to halo stellar streams. Several much longer fireballs (lengths of 5–8 kpc) are also observed, especially in the northern regions of the tail, that may be in an older evolutionary stripping phase. The small fireballs

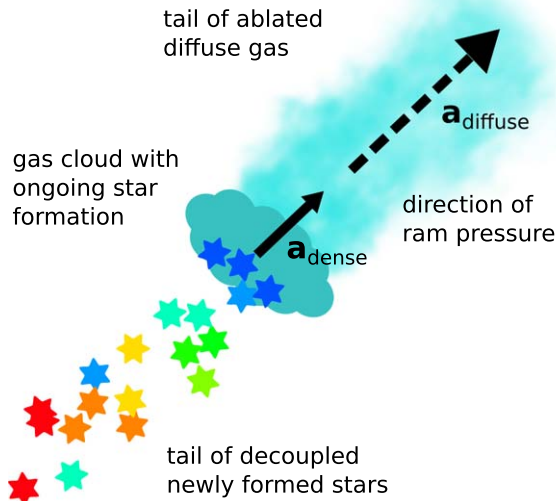


**Figure 7.** Schematic of the double-sided fireball model, with a tail of newly born stars pointing toward the galaxy, decoupled from the outwardly accelerating gas cloud, and another tail of diffuse gas ablated by ram pressure from the denser cloud extending in the opposite direction. The diffuse gas with a lower surface density is accelerated more than the dense gas (as indicated by the arrows). In this simple scenario, an age gradient would form along the stellar tail, but further fragmentation and cooling/collapse of the decoupled star-forming dense clumps may complicate it.

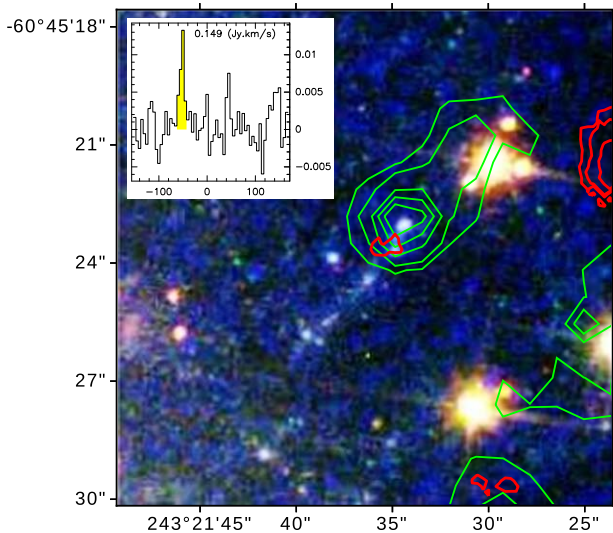


**Figure 8.** Example of a double-sided fireball in an *HST* image with H $\alpha$  (green) and CO (red) contours overlaid. The feature consists of a compact H II region associated with weak CO emission, a stellar tail pointing toward the galaxy, and a tail of more diffuse H $\alpha$  emission extending in the opposite direction. The CO contour levels are 0.1, 0.15, 0.24, and 0.39 Jy beam $^{-1}$  km s $^{-1}$ . The displayed region is  $\sim 12'' \times 12''$ . The inset panel shows the spectrum of the central associated CO emission region.

offset) weak CO clump at the head of a small fireball with a diffuse tail extending along the direction of the wind. It is located in the northern component of the tail, close to the main galaxy. The associated CO emission region has an H $_2$  mass of  $\sim 2.4 \times 10^6 M_{\odot}$ . More similar structures (though less clear and without detected associated CO clumps) may be found mainly in the southern tail component.

are likely dynamically young structures ( $\sim 10$  Myr), while their larger relatives have ages of  $\sim 50$  Myr.

We found that some linear  $H\alpha$  features, compact  $H\alpha$ -emitting clumps, and young star regions may be interconnected into double-sided fireballs. We propose a simple scenario based on dynamical separation of gas phases in which denser gas clumps pushed by ram pressure form stars that decouple from the clumps and create inward-pointing stellar tails, while at the same time, the clumps are ablated by the strong ram pressure, and tails of diffuse gas are formed in the opposite direction to the stellar tails.



This paper makes use of the following ALMA data: ADS/JAO.ALMA#2015.1.01520.S. ALMA is a partnership of the ESO (representing its member states), NSF (USA), and NINS (Japan), together with the NRC (Canada), MOST and ASIAA (Taiwan), and KASI (Republic of Korea), in cooperation with the Republic of Chile. The Joint ALMA Observatory is operated by the ESO, AUI/NRAO, and NAOJ. This research has made use of the HyperLeda database (<http://leda.univ-lyon1.fr>).

We thank Jonathan Braine, the referee of the paper, for helpful comments that improved the quality of this paper substantially. P.J. acknowledges support through project LM2015067 of the Ministry of Education, Youth and Sports of the Czech Republic. P.J. and J.P. acknowledge support from the project 19-18647S of the Czech Science Foundation and from the institutional research project RVO:67985815. M.S. acknowledges support from NASA grants GO6-17111X and 80NSSC18K0606 and NSF grant 1714764. L.C. is the recipient of an Australian Research Council Future Fellowship (FT180100066) funded by the Australian Government. T.S. acknowledges support through fellowship SFRH/BPD/103385/2014 funded by FCT (Portugal) and POPH/FSE (EC). This work was supported by Fundação para a Ciência e a Tecnologia (FCT) through national funds (UID/FIS/04434/2013) and by FEDER through COMPETE2020 (POCI-01-0145-FEDER-007672). T.S. also acknowledges support from DL 57/2016/CP1364/CT0009. This work was supported by FCT/MCTES through national funds (PIDDAC) by grant PTDC/FIS-AST/29245/2017. E.B. acknowledges support from the UK Science and Technology Facilities Council (grant No. ST/M001008/1). M.F. acknowledges support by the Science and Technology Facilities Council (grant No. ST/P000541/1). This project has received funding from the European Research Council (ERC) under the European Union's Horizon 2020 research and innovation program (grant agreement No. 757535).

*Facility:* ALMA.

*Software:* CASA (McMullin et al. 2007), GILDAS (Guiloteau & Lucas 2000), astropy (Astropy Collaboration et al. 2013).

## ORCID iDs

Pavel Jáchym  <https://orcid.org/0000-0002-1640-5657>  
 Ming Sun  <https://orcid.org/0000-0001-5880-0703>  
 Françoise Combes  <https://orcid.org/0000-0003-2658-7893>  
 Luca Cortese  <https://orcid.org/0000-0002-7422-9823>  
 Suresh Sivanandam  <https://orcid.org/0000-0002-0767-8135>  
 Elias Brinks  <https://orcid.org/0000-0002-7758-9699>  
 Jan Palouš  <https://orcid.org/0000-0001-6729-2851>  
 Michele Fumagalli  <https://orcid.org/0000-0001-6676-3842>

## References

- Abramson, A., Kenney, J. D. P., Crowl, H. H., et al. 2011, *AJ*, 141, 164  
 Abramson, A., Kenney, J., Crowl, H., & Tal, T. 2016, *AJ*, 152, 32  
 Astropy Collaboration, Robitaille, T. P., Tollerud, E. J., et al. 2013, *A&A*, 558, A33  
 Banda-Barragán, W. E., Zertuche, F. J., Federrath, C., et al. 2019, *MNRAS*, 486, 4526  
 Bertoldi, F., & McKee, C. F. 1992, *ApJ*, 395, 140  
 Boehringer, H., Neumann, D. M., Schindler, S., et al. 1996, *ApJ*, 467, 168  
 Bolatto, A. D., Wolfire, M., & Leroy, A. K. 2013, *ARA&A*, 51, 207  
 Boselli, A., Fossati, M., Ferrarese, L., et al. 2018, *A&A*, 614, A56  
 Boselli, A., Cuillandre, J. C., Fossati, M., et al. 2016, *A&A*, 587, A68  
 Catinella, B., Saintonge, A., Janowiecki, S., et al. 2018, *MNRAS*, 476, 875  
 Chung, A., van Gorkom, J. H., Kenney, J. D. P., Crowl, H., & Vollmer, B. 2009, *AJ*, 138, 1741  
 Chung, A., van Gorkom, J. H., Kenney, J. D. P., & Vollmer, B. 2007, *ApJL*, 659, L115  
 Combes, F., Dupraz, C., Casoli, F., et al. 1988, *A&A*, 203, L9  
 Cooper, J. L., Bicknell, G. V., Sutherland, R. S., & Bland-Hawthorn, J. 2009, *ApJ*, 703, 330  
 Cortese, L., Gavazzi, G., Boselli, A., et al. 2006, *A&A*, 453, 847  
 Cortese, L., Marcellac, D., Richard, J., et al. 2007, *MNRAS*, 376, 157  
 Cramer, W. J., Kenney, J. D. P., Sun, M., et al. 2019, *ApJ*, 870, 63  
 Dasysra, K. M., Combes, F., Salomé, P., et al. 2012, *A&A*, 540, A112  
 Ebeling, H., Stephenson, L. N., & Edge, A. C. 2014, *ApJL*, 781, L40  
 Elmegreen, D. M., Elmegreen, B. G., Chromey, F. R., & Fine, M. S. 2000, *AJ*, 120, 733  
 Finoguenov, A., Briel, U. G., Henry, J. P., et al. 2004, *A&A*, 419, 47  
 Fossati, M., Gavazzi, G., Boselli, A., & Fumagalli, M. 2012, *A&A*, 544, A128  
 Fossati, M., Fumagalli, M., Boselli, A., et al. 2016, *MNRAS*, 455, 2028  
 Fumagalli, M., Gavazzi, G., Scaramella, R., & Franzetti, P. 2011, *A&A*, 528, A46  
 Fumagalli, M., Fossati, M., Hau, G. K. T., et al. 2014, *MNRAS*, 445, 4335  
 Gavazzi, G., Boselli, A., Mayer, L., et al. 2001, *ApJL*, 563, L23  
 George, K., Poggianti, B. M., Gullieuszk, M., et al. 2018, *MNRAS*, 479, 4126  
 Gronke, M., & Oh, S. P. 2018, *MNRAS*, 480, L111  
 Gullieuszk, M., Poggianti, B. M., Moretti, A., et al. 2017, *ApJ*, 846, 27  
 Gunn, J. E., & Gott, J. R., III 1972, *ApJ*, 176, 1  
 Guilloteau, S., & Lucas, R. 2000, Imaging at radio through submillimeter wavelengths, Astronomical Society of the Pacific Conf. Series, Vol. 217 ed. J. G. Mangum & S. J. E. Radford., 299  
 Hester, J. A., Seibert, M., Neill, J. D., et al. 2010, *ApJL*, 716, L14  
 Jáchym, P., Combes, F., Cortese, L., Sun, M., & Kenney, J. D. P. 2014, *ApJ*, 792, 11  
 Jáchym, P., Sun, M., Kenney, J. D. P., et al. 2017, *ApJ*, 839, 114  
 Kauffmann, J., Pillai, T., & Goldsmith, P. F. 2013, *ApJ*, 779, 185  
 Kenney, J. D. P., van Gorkom, J. H., & Vollmer, B. 2004, *AJ*, 127, 3361  
 Kenney, J. D. P., Geha, M., Jáchym, P., et al. 2014, *ApJ*, 780, 119  
 Klein, R. I., McKee, C. F., & Colella, P. 1994, *ApJ*, 420, 213  
 Koopmann, R. A., & Kenney, J. D. P. 2004, *ApJ*, 613, 866  
 Köppen, J., Jáchym, P., Taylor, R., & Palouš, J. 2018, *MNRAS*, 479, 4367  
 Lee, B., & Chung, A. 2018, *ApJL*, 866, L10  
 Lee, B., Chung, A., Tonnesen, S., et al. 2017, *MNRAS*, 466, 1382  
 Leroy, A. K., Walter, F., Bigiel, F., et al. 2009, *AJ*, 137, 4670  
 Machacek, M., Dosaj, A., Forman, W., et al. 2005, *ApJ*, 621, 663  
 Mattern, M., Kainulainen, J., Zhang, M., & Beuther, H. 2018, *A&A*, 616, A78  
 McMullin, J. P., Waters, B., Schiebel, D., Young, W., & Golap, K. 2007, CASA architecture and applications, in Proc. Astronomical Data Analysis Software and Systems XVI, Vol. 376, ed. R. A. Shaw, F. Hill, & D J Bell, 127  
 Moretti, A., Paladino, R., Poggianti, B. M., et al. 2018, *MNRAS*, 480, 2508  
 Nehlig, F., Vollmer, B., & Braine, J. 2016, *A&A*, 587, A108  
 Oosterloo, T., & van Gorkom, J. 2005, *A&A*, 437, L19  
 Pety, J., Schinnerer, E., Leroy, A. K., et al. 2013, *ApJ*, 779, 43  
 Poggianti, B. M., Moretti, A., Gullieuszk, M., et al. 2017, *ApJ*, 844, 48  
 Poggianti, B. M., Gullieuszk, M., Tonnesen, S., et al. 2019, *MNRAS*, 482, 4466  
 Quilis, V., Moore, B., & Bower, R. 2000, *Sci*, 288, 1617  
 Scott, T. C., Brinks, E., Cortese, L., Boselli, A., & Bravo-Alfaro, H. 2018, *MNRAS*, 475, 4648  
 Scott, T. C., Usero, A., Brinks, E., et al. 2015, *MNRAS*, 453, 328  
 Scott, T. C., Cortese, L., Brinks, E., et al. 2012, *MNRAS*, 419, L19  
 Scott, T. C., Bravo-Alfaro, H., Brinks, E., et al. 2010, *MNRAS*, 403, 1175  
 Sivanandam, S., Rieke, M. J., & Rieke, G. H. 2010, *ApJ*, 717, 147  
 Smith, R. J., Lucey, J. R., Hammer, D., et al. 2010, *MNRAS*, 408, 1417

- Solomon, P. M., & Vanden Bout, P. A. 2005, *ARA&A*, 43, 677
- Sun, M., Donahue, M., Roediger, E., et al. 2010, *ApJ*, 708, 946
- Sun, M., Donahue, M., & Voit, G. M. 2007, *ApJ*, 671, 190
- Sun, M., Jones, C., Forman, W., et al. 2006, *ApJL*, 637, L81
- Sun, M., & Vikhlinin, A. 2005, *ApJ*, 621, 718
- van Gorkom, J. H. 2004, *Clusters of Galaxies: Probes of Cosmological Structure and Galaxy Evolution* (Cambridge: Cambridge University Press), 305
- Vantyghem, A. N., McNamara, B. R., Russell, H. R., et al. 2019, *ApJ*, 870, 57
- Verdugo, C., Combes, F., Dasyra, K., Salomé, P., & Braine, J. 2015, *A&A*, 582, A6
- Vollmer, B., Braine, J., Pappalardo, C., & Hily-Blant, P. 2008, *A&A*, 491, 455
- Vollmer, B., Braine, J., Combes, F., et al. 2005, *A&A*, 441, 473
- Vollmer, B., Braine, J., Balkowski, C., Cayatte, V., & Duschl, W. J. 2001a, *A&A*, 374, 824
- Vollmer, B., Cayatte, V., van Driel, W., et al. 2001b, *A&A*, 369, 432
- Wang, Q. D., Owen, F., & Ledlow, M. 2004, *ApJ*, 611, 821
- Woudt, P. A., Kraan-Korteweg, R. C., Lucey, J., et al. 2008, *MNRAS*, 383, 445
- Yagi, M., Komiyama, Y., Yoshida, M., et al. 2007, *ApJ*, 660, 1209
- Yagi, M., Yoshida, M., Komiyama, Y., et al. 2010, *AJ*, 140, 1814
- Yagi, M., Gu, L., Fujita, Y., et al. 2013, *ApJ*, 778, 91
- Yoshida, M., Yagi, M., Komiyama, Y., et al. 2008, *ApJ*, 688, 918
- Yoshida, M., Ohyama, Y., Iye, M., et al. 2004, *AJ*, 127, 90
- Yoshida, M., Yagi, M., Komiyama, Y., et al. 2012, *ApJ*, 749, 43
- Zabel, N., Davis, T. A., Smith, M. W. L., et al. 2019, *MNRAS*, 483, 2251